Chapter 2

The pulsatile 3D-Hemodynamics in a doubly afflicted human descending abdominal artery with iliac branching

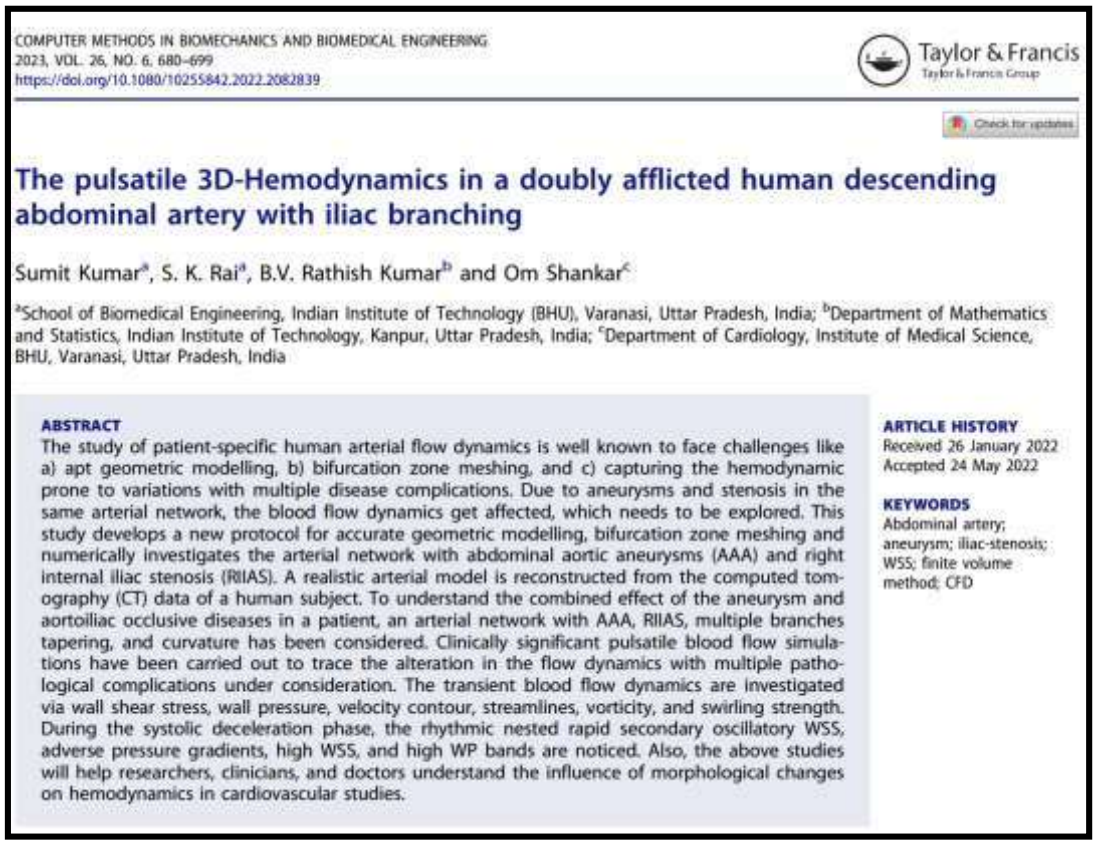

COMPUTER METHODS IN BIOMECHANICS AND BIOMEDICAL ENGINEERING
2023, VOL. 26, NO. 6, 680–699
https://doi.org/10.1080/10255842.2022.2082839

Taylor & Francis
Taylor & Francis Group

Check for updates

The pulsatile 3D-Hemodynamics in a doubly afflicted human descending abdominal artery with iliac branching

Sumit Kumar[a], S. K. Rai[a], B.V. Rathish Kumar[b] and Om Shankar[c]

[a]School of Biomedical Engineering, Indian Institute of Technology (BHU), Varanasi, Uttar Pradesh, India; [b]Department of Mathematics and Statistics, Indian Institute of Technology, Kanpur, Uttar Pradesh, India; [c]Department of Cardiology, Institute of Medical Science, BHU, Varanasi, Uttar Pradesh, India

ABSTRACT

The study of patient-specific human arterial flow dynamics is well known to face challenges like a) apt geometric modelling, b) bifurcation zone meshing, and c) capturing the hemodynamic prone to variations with multiple disease complications. Due to aneurysms and stenosis in the same arterial network, the blood flow dynamics get affected, which needs to be explored. This study develops a new protocol for accurate geometric modelling, bifurcation zone meshing and numerically investigates the arterial network with abdominal aortic aneurysms (AAA) and right internal iliac stenosis (RIIAS). A realistic arterial model is reconstructed from the computed tomography (CT) data of a human subject. To understand the combined effect of the aneurysm and aortoiliac occlusive diseases in a patient, an arterial network with AAA, RIIAS, multiple branches tapering, and curvature has been considered. Clinically significant pulsatile blood flow simulations have been carried out to trace the alteration in the flow dynamics with multiple pathological complications under consideration. The transient blood flow dynamics are investigated via wall shear stress, wall pressure, velocity contour, streamlines, vorticity, and swirling strength. During the systolic deceleration phase, the rhythmic nested rapid secondary oscillatory WSS, adverse pressure gradients, high WSS, and high WP bands are noticed. Also, the above studies will help researchers, clinicians, and doctors understand the influence of morphological changes on hemodynamics in cardiovascular studies.

ARTICLE HISTORY
Received 26 January 2022
Accepted 24 May 2022

KEYWORDS
Abdominal artery; aneurysm; iliac-stenosis; WSS; finite volume method; CFD

Chapter 2

The pulsatile 3D-Hemodynamics in a doubly afflicted human descending abdominal artery with iliac branching

2.1 Introduction

One of the primary causes of blood flow abnormalities and premature deaths worldwide are cardiovascular diseases (CVDs). Recent CVDs data from WHO indicates that more than 17.8 million people succumb to this disease every year ("Cardiovascular diseases (CVDs)," n.d.). Atherosclerosis is a disease in which plaque (made up of fat, cholesterol, calcium, and other substances found in the blood) forms inside the arteries in the human cardiovascular system. Because of the continuous deposition of plaque over a period, it hardens and narrows the lumen of the arteries. It affects the flow of oxygen-rich blood to the organs and other parts of the lower extremities (Dwidmuthe et al., 2020; ,Tsubota et al., 2006; Vorp, 2009). The abdominal aorta is the primary and largest artery originating from the left ventricle and extends to the pelvic region. It splits into two bifurcations i.e. common iliac bifurcations (internal and external). It has intricate shapes, including non-planar curvature, bifurcations at proximal (arch of the aorta), distal (common iliac bifurcations), infrarenal aorta, suprarenal aorta and significant narrowing with dilatable vessel walls. Fry , Caro et al, Ku and Boutsianis (Boutsianis et al., 2009b; Fry, n.d.; Ku and Woodruff, 1997; Vasava et al., 2012) have stated that the intricate geometries of the abdominal aorta make it sensitive to the aneurysm and atherosclerotic lesions. Two of the major arterial diseases in the cardiovascular system are abdominal aortic

aneurysm (AAA) and lower extremity arterial disease (LEAD), like right internal iliac artery stenosis (RIIAS) (Mahé et al., 2015; Wong et al., 2012). AAA are localized broadening of the abdominal aorta such that the diameter 'd' > 3 cm or 50% larger than the normal artery. Also, it is asymptomatic, which is not easily detectable on physical examination, and it remains until not discovered by the radiologist using computed tomography (CT) or magnetic resonance imaging (MRI) imaging (Aulivola, 2008; Mahé et al., 2015). The occurrence of AAA is mainly in those over 50 years old, in men, and among those with a family history. It is also a well-known fact that an aneurysm ruptures when the stress acting on the arterial wall exceeds its failure limit. According to Laplace empirical relations, wall stress is directly proportional to its intraluminal pressure and radius. Stenosis occurs because of plaque formation, and these plaques damage the endothelium layer of the artery, due to which walls become calcified, thick and fibrotic, and the arterial lumen narrow (Gay and Zhang, 2009). It has been noticed that 20% to 60% of LEAD patients are asymptomatic (Kelsey et al., 2016; Mahé et al., 2015). Patients having RIIAS usually report a steady reduction in their walking ability, which is estimated by the maximal walking distance (Kelsey et al., 2016; Sumner, 1988). According to literature, it has been noticed that although AAA and RIIAS are not ideal cylinders in shape, Laplace's law still applies. The presence of aneurysms and stenosis in the same artery can lead to the development of undesirable adverse pressure gradient and shear stress oscillation during the cardiac cycle. In a compounded disease condition such as the joint presence of AAA and RIIAS in the same artery, the resulting flow complexities are more severe and has not been addressed. Hence, it is essential to study such pathological complexities with AAA & RIIAS in the same artery or arterial network.

Since the last decade, many studies have been carried out for transient blood flow dynamics on both idealized and patient-specific reconstructed models of aortic arch from CT scan (Huang et al., 2010; Piskin and Serdar Celebi, 2013; Tian et al., 2013; Vasava, 2011). In these hemodynamic studies, it was observed that the distribution of oscillatory and low WSS are significant factors in rising atherosclerotic plaques. L.J. Kelsey et al. (Kelsey et al., 2016) and N. Pinho, C.F. Castro, et al. (Pinho et al., 2019b, 2019a) investigated the impact of cross-sectional area, angles between the common trunk and the side-branches, tortuosity and bends in in right and left coronary ateries their influence on hemodynamic descriptors. Narrowing of the arterial lumen is stated in terms of percentage severity of stenosis. A severity of 91% means only 9% opening area is available for the blood flow through the artery in the stenosed region. Some researchers studied in-vitro the steady-state blood flow through a stenosed vessel, while some treated it to be pulsatile (Ahmed and Giddens, 1983; Siouffi et al., 1984; Tabe et al., 2011). For three-dimensional subject-specific detailed hemodynamic analysis, medical image acquisition considering CT or MRI scan, image classification, computer-aided design of blood vessels and CFD studies play a significant role. Many research works have been carried out on modelling and simulation of the cardiovascular system using medical imaging data and CFD (Doost et al., 2015; Harita and Anburajan, 2013; Huang et al., 2010; Javadzadegan et al., 2014; Jozwik and Obidowski, 2010; Karimi et al., 2014a; kumar and Deoghare, 2018; Nowak et al., 2019; Raptis et al., 2022; Tripathi et al., 2021; Volpi et al., 2009). The common finding in all studies is that destruction of blood cells due to oscillatory WPs, WSSs, CVD triggered abnormal variations in arterial lumen dimensions, recirculating cum stagnant flow zone with high shear stress variation etc., are the main factors in developing

plaques and aneurysms. Further, these hemodynamic factors are sensitive to morphological changes in blood vessels due to multiple pathological complexities. For instance, it has been reported that the distribution of reversed flow and WSS are the main factors for the morphological variations in the blood vessel leading to the growth of stenosis and aneurysms (Alishahi et al., 2011; Gay and Zhang, 2009). Hence the presence of multiple such complexities can lead to much more involved and subtle variation in hemodynamics and need special attention.

Despite the enormous amount of work on patient-specific and idealized geometry-based blood flow simulation in healthy and unhealthy arteries, there is hardly any reporting on numerical investigation of flow in vessels with multiple cardiovascular diseases like AAA and RIIAS. Therefore, to enrich and strengthen the clinical diagnostic information relevant to the complex arterial pathology, an effort has been made to study the blood flow dynamics in a realistic 3D model of an artery having both AAA and RIIAS based on CT/MRI subject data.

In this study, the medical imaging tools like contrasting, segmentation, thresholding, morphological operation and contour adjustment techniques have been effectively and efficiently used on the CT data of the subject to arrive at an accurate 3D geometric model. Also, to reduce the calculation time of simulation, a new meshing protocol, i.e., local meshing, selection of suitable mesh element size and shape at a desired region of interest where the result has to be more precise and accurate, has been employed.

The present work presents (i) an accurate geometric modelling and localized meshing of AAA and RIIAS compounded in the same artery and (ii) a detailed visualization of

transient flow dynamics at various cardiac time steps with physiologically/clinically measured pulsatile input data. By employing patient-specific CT scan data, a healthy abdominal artery is designed first. By adopting the available design data for aneurysms and stenosis, a new model of an artery is designed. This model includes one inlet and nine different outlets consisting of AAA and RIIAS. The impact of combined AAA and RIIAS complexity is examined through WSS, vorticity, swirling strength, velocity contour, streamlines, and velocity vector and are described under the results. The numerical simulations are presented to support cardiologists with diagnostic tools with enhanced and deeper inference capabilities in medicine. The present methodology and rigorous parametric studies of WSS, velocity contour could assist doctors or practitioners in forecasting whether the deposition of plaque and AAA is controlled or growing. This will help in the early diagnosis and treatment of aneurysm (e.g., AAA) compounded by stenosis (e.g., RIIAS) in a complex arterial network with several branches.

2.2 Methods

A new methodology for accurate 3D geometrical modelling of patient-specific geometry using CT-scan in DICOM image format, meshing and CFD simulation is designed and illustrated in (Figure 2.1). The details of each methodology are described in the following subsections. (Figure 2.1) depicts a step-by-step procedure for numerical simulation of complex geometry with patient-specific data. The first step includes pre-processing, i.e., three-dimensional geometry modelling using CT-scan DICOM data of a patient. It includes (i) contrasting, i.e., adjustment of image intensity for clear visualization of soft tissue in the dataset, (ii) segmentation, i.e., partitioning

an image into various segments to locate objects (soft and hard tissue), (iii) boundaries in the image, (iv) morphological operation, i.e., dilation (adding a pixel to boundaries of objects in the image), (v) erosion, i.e. (removing small objects and retaining substantive objects) and (vi) some smoothing operation across bifurcations. The next step after three-dimensional modelling is (a) meshing which is followed by (b) selection of suitable material, (c) boundary conditions setup and (d) solver physics setup for simulation. The last step is post-processing which includes (i) result extraction, (ii)analysis of simulation at various time steps of the cardiac cycle and (iii) validation.

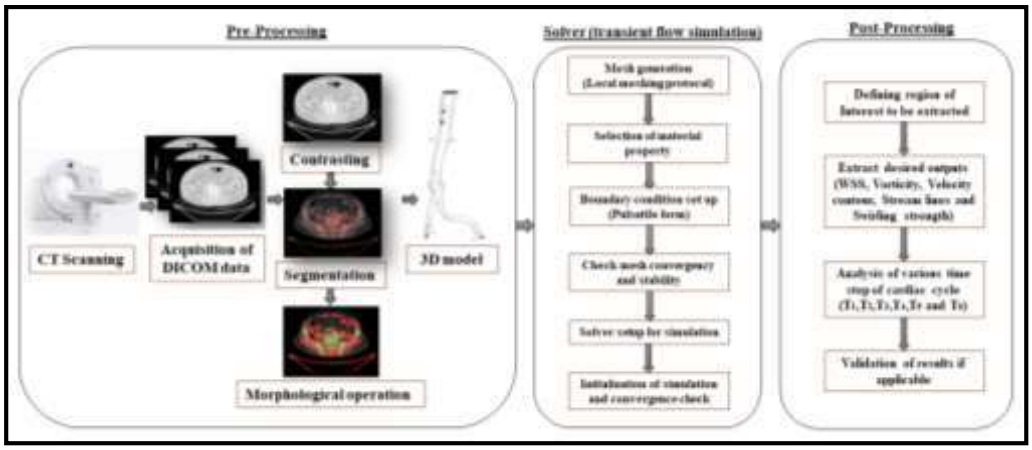

Figure 2.1 : Methodology designed for transient CFD simulation with step-by-step process description from Pre-processing, solver and Post Processing.

2.2.1 Geometric model

A three-dimensional patient-specific model of AAA lumen shape is designed from an abdomen CT- scan of an 80-year-old male from (128 slices, GE medical system, CT scan centre, IMS BHU, Varanasi, India). For patient-specific data acquisition, the patient has given informed consent and ethical permission is taken from the radiology

department, Institute of medical science BHU, Varanasi, India. During image acquisition, the volunteer did not suffer from any hardships. The protocol used for image acquisition (6.1 abdomens 5mm new). The scanning was performed from the aorta region to the lower abdomen portion with 512×512-image matrices, 0.9609 mm of pixel size, and 1.25 mm thickness. The medical image modelling tool "Materialize MIMICS V18" is used in designing the 3D model from the obtained patient-specific 2D-DICOM image slice data. The details of the scanned data are described in Tables (2.1 & 2.2). Firstly, a healthy 3D model of the artery is designed as a reference then it is converted into a diseased one, consisting of AAA & RIIAS. The aneurysm (AAA of 47%) and stenosis (RIIAS of 91%) are compounded together in the same arterial geometry, setting the design parameters D/L_a (Diameter of artery/length of aneurysm) to 0.47 and D/L_s (Diameter of artery/length of stenosis) to 0.91 respectively (Aggarwal et al., 2011; Isselbacher, 2005).

To analyze hemodynamic in the designed 3D complex arterial network model, considered several cross-sections across the region of interest of the arterial network, as illustrated in (Figure 2.2). These cross-sections (S_1 to S_{12}) have been carefully selected to avoid the artefacts of boundary conditions as these are away from the inlet and outlets. The axial, coronal and sagittal views of the reconstructed 3D model are presented in (Figure. 2.2). The space claim module of ANSYS (2021R2) workbench has been used to convert the base geometry from its unstructured triangulated surface format (STL), as given by the MIMICS modelling tool, to the solid form as required for computational flow simulations. It is to be noted that for the arterial network under

consideration, the physiologically established Reynolds number is in the range of 1400-1600 at peak systolic phase and in the range of 300-500 at diastolic phase.

Table 2.1. CT scan slice information's

Geometrical parameters	Values Measured
Pixel size	0.9609 mm
Image Resolution	512*512 pixels
Number of DICOM slices	128
Image width	85.5469 mm
Image height	65.0024 mm
Slice thickness	1.25 mm

Table 2.2. Dimensional details of geometry

Geometrical Parameters	Values Measured
Length of the Artery	220 mm
Diameter of Inlet	23.76 mm
Diameter of Outlet1	5.78 mm
Diameter of Outlet2	5.26 mm
Diameter of Outlet3	4.36 mm
Diameter of Outlet4	3.7 mm
Diameter of Outlet5	1.7 mm
Diameter of Outlet6	7.6 mm
Diameter of Outlet7	5.3 mm
Diameter of Outlet8	5.82 mm
Diameter of Outlet9	2.84 mm

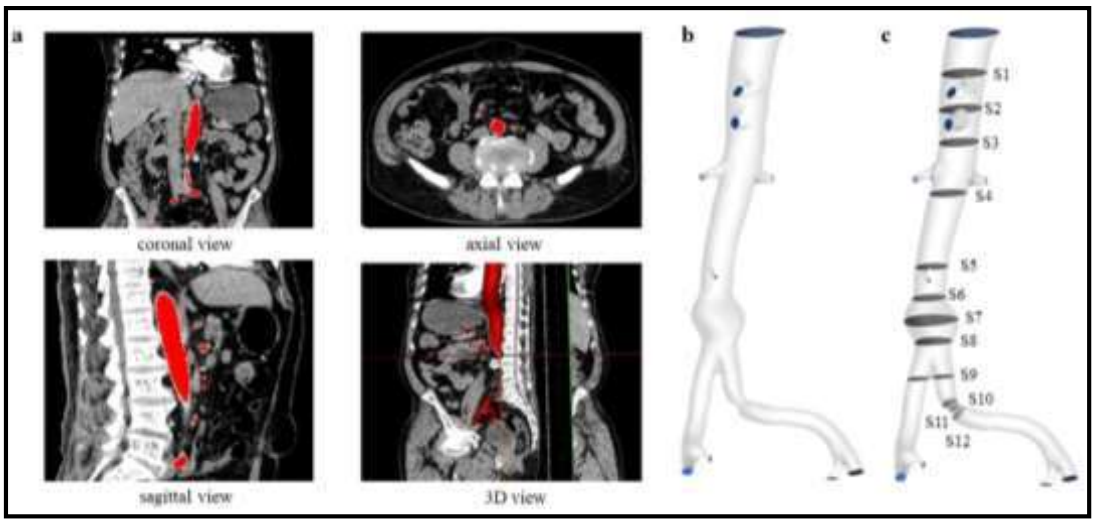

Figure 2.2 : Reconstruction of the three-dimensional model using CT-scan DICOM image (a) segmentation of region of interest in axial view, coronal view & sagittal view (b) 3D model of artery (c) Various sectional place considered in AAA and RIIAS region.

2.2.2 Discretization and mesh independency check

The geometry is meshed using the novel local mesh methodology as shown in (Figure 2.3), and mesh parameters are described in Table 2.3. In local meshing, firstly, the local coordinates are set for selecting respective spheres of influence in regions that need to have meshed locally. Later, using sizing operation, all the designated local zones under the spheres of influence have been meshed, as shown in (Figure 2.3). From literature related to the image-based intricate shapes, a tetrahedral element is known to be one of the best fits (Boutsianis et al., 2009b; Frauenfelder et al., 2006). Hence, the tetrahedral elements are considered for meshing in this model. To obtain better and precise results near artery wall, five inflation layers are set up with a growth rate of 1.2. A detailed view of the mesh is available in (Figure 2.4).

For the grid independency test, three mesh element sizes of 3mm, 2mm and 1mm have been used respectively for coarse, moderate and fine mesh generations. The mesh parameters for the grid independence test are given in Table 2.3. For the grid independency test, a check on the maximum velocity at nine outlets in all three different mesh models is used, and the outcome of the test is shown in (Figure 2.5). All the numerical simulations are carried out on fine mesh with 1358804 number of nodes, and 5513363 number of elements as less than 1% variation in the maximum velocities at all the nine outlets is noticed, as we move from moderate grid to fine grid.

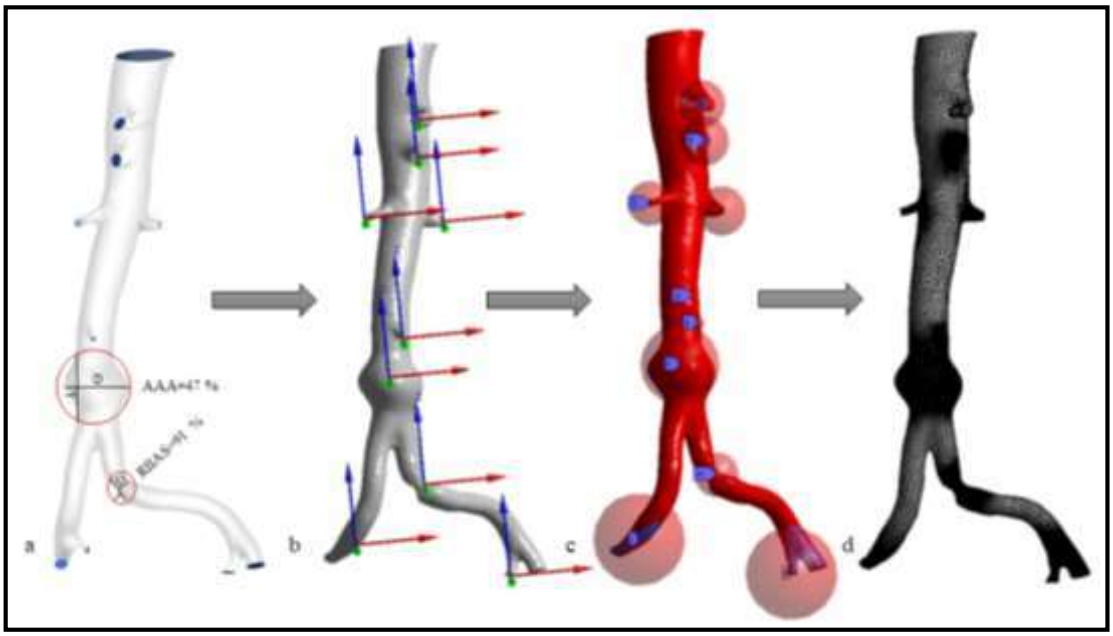

Figure 2.3 : Strategy adopted for local meshing (a) 3D model of artery (b) Selection of local coordinates for meshing (c) Selection of spherical mesh lobe to restrict the local mesh volume (d) final mesh model

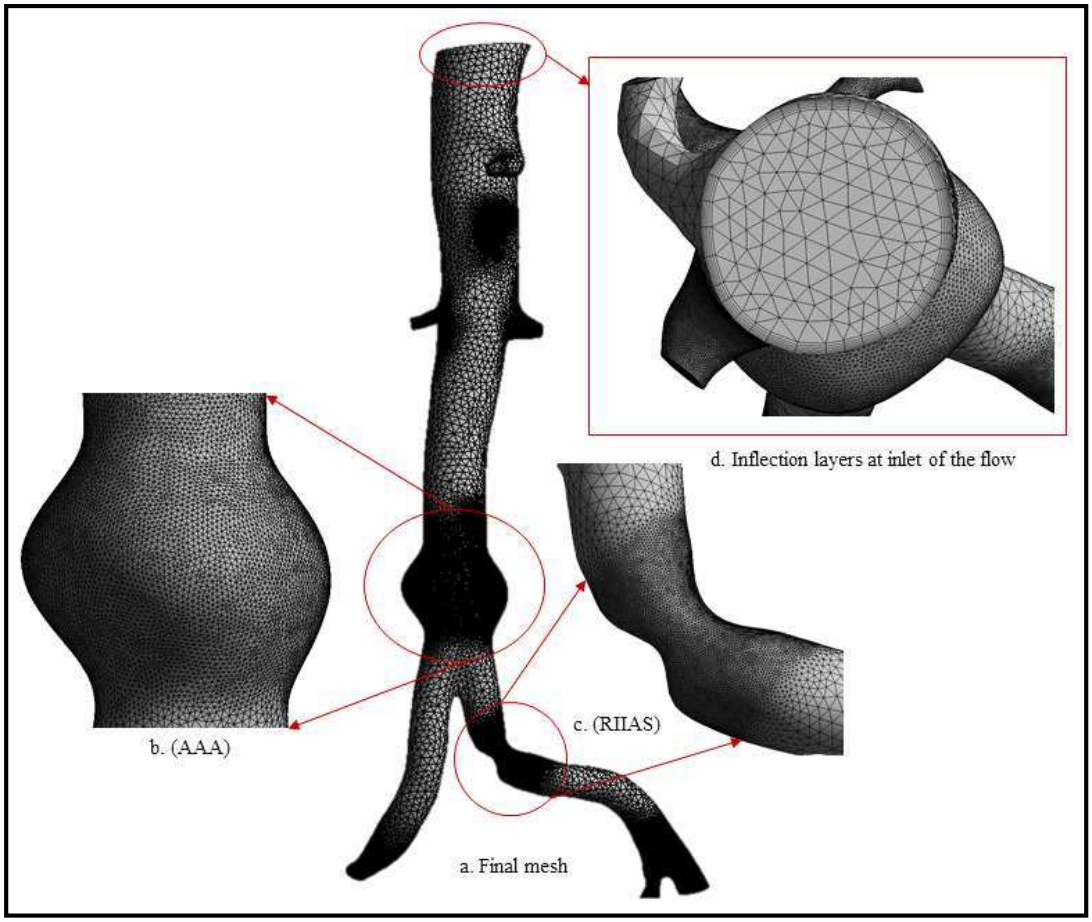

Figure 2.4 : Mesh model of: (a) whole domain, (b) different sizes of surface element for AAA and (c) different sizes of surface element for RIIAS (d) the cross-section of the artery different with densities of the mesh in the section

Table 2.3. Mesh Independency Check parameter

Mesh sizes	Number of Elements	Number of nodes
Mesh1 (1mm size)	5513363	1358804
Mesh2 (2 mm size)	3054057	796934
Mesh3 (3 mm size)	2740574	712229

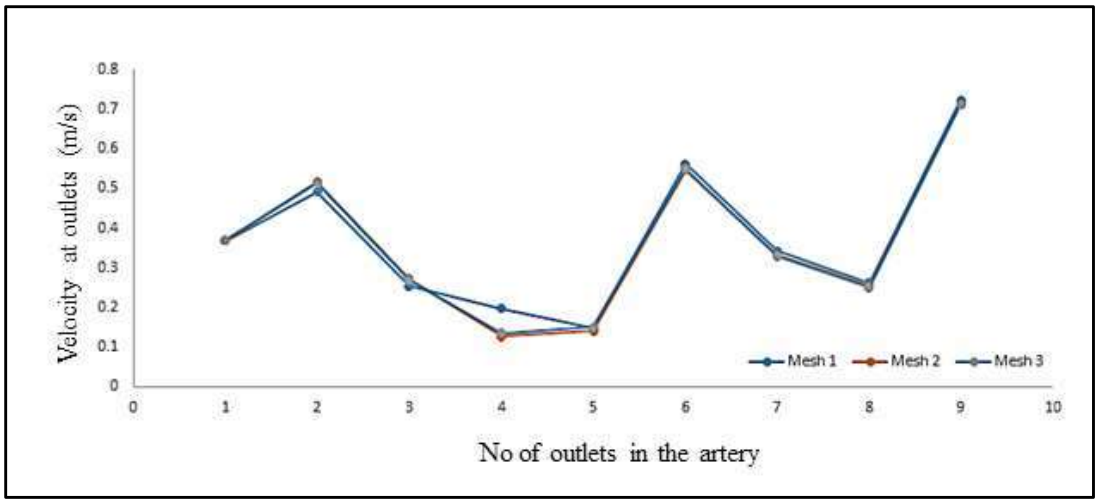

Figure 2.5 : Mesh independency test using different mesh size of mesh1, mesh 2 & and mesh 3 at different outlets

2.2.3 Computational methods

Finite Volume Method under ANSYS – FLUENT fluid flow solver is used for investigating computational blood flow dynamics in the human descending aorta with AAA, RIIAS and multiple branches. For CFD simulations, blood flow is assumed to be Newtonian, laminar, single-phased, and transient. The transient fluid flow governing equations under these assumptions are expressed below in Eq. (1) and (2).

2.2.4 Governing equations for blood flow simulation

The equations governing the conservation of mass and momentum for Newtonian incompressible fluid flow are given by:

$$\nabla . u = 0 \qquad (1)$$

$$\rho \left[\frac{\partial u}{\partial t} + (u.\nabla)u\right] = -\nabla p - \nabla . \tau \qquad (2)$$

Where u is the velocity vector, t is the time, ρ is the fluid density, p is hydrostatic pressure, and τ is shear stress, and it is defined by:

$$\tau = \mu(\nabla u + (\nabla u)^t)$$

where μ is the coefficient of dynamic viscosity.

2.2.5 Simulation setup

No-slip boundary conditions are implemented on the vessel walls, which are treated to be non-compliant. In case of patient specific blood flow modelling and simulations outlet boundary conditions are always the most difficult to set for realism in such CFD analyses. Here normal person flow information taken from literature as a stress-free boundary conditions which is the most convenient though mot most realistic. In this case the inlet velocity profile is a pulsatile function of time (Figure 2.6), based on the realistic human data from clinical setup, and the same has been used by (Karimi et al., 2014b). The stress-free outflow boundary condition is applied at all the outlets of the descending abdominal arterial network with bifurcations as suggested and depicted by (Karimi et al., 2014a). The spatial discretization of the velocity-pressure coupling is carried out following the SIMPLE algorithm with a second-order upwind scheme for convective terms and a cell-based approximation for pressure gradients. A workstation of 48 cores with 64 GB RAM and an 8 GB graphics card is used to carry out the CFD simulations. For precise controls of velocity field near the artery walls, a fine grid with a thickness of 0.1 mm and a growth rate of 1.2 is used near the vessel wall. A localized meshing technique with 0.25 mm element size is used at various local coordinates. The transient flow analysis is carried out using the first-order implicit Euler method with a

time step of size 0.01 ms. The convergence threshold values for the residuals are set at 10^{-4} for all equations, and it provided well-converged results at each of the time steps. All the simulations in the present work are carried out for at least three cardiac cycles till a periodic state in the solution has been reached. Flow simulation results for one complete cycle is presented and discussed in the next section.

2.3 Results and discussion

The cardiac flow cycle consists of two phases. The first phase, wherein the flow gets accelerated, is known as the systolic phase, and the second phase, during which the flow is decelerating, is known as the diastolic phase. Results at different time instances, as shown below, are traced to unravel the transient blood flow dynamics:

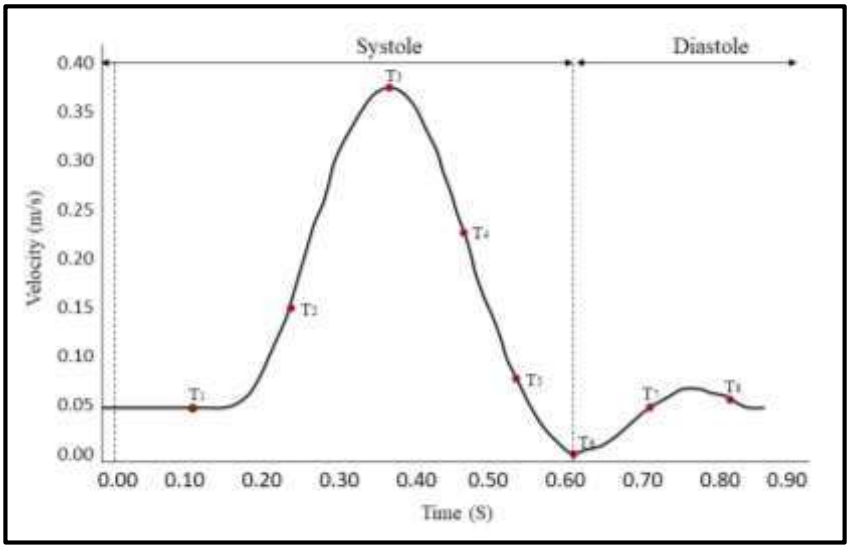

Figure 2.6 : Pulsatile velocity inlet profile

- T_1 = 0.1 s at the start of the systole and late of diastole instant
- T_2 =0.2 s at the mid accelerating phase of systole
- T_3 =0.3 s at peak systole

- T_4 =0.4 s at the middle of the decelerating systolic phase with the same velocity as T_2
- T_5 =0.5 s at the end of the decelerating phase of systole
- T_6 =0.6 s at the start of the diastole instant

CT-image based patient-specific blood flow analysis of healthy human abdominal artery is simulated first to analyze the healthy blood flow dynamics under Newtonian flow conditions. Later the same is repeated for the pathological arterial system with AAA and RIIAS. Blood flow dynamics in terms of Wall Shear Stress (WSS), Wall Pressure (WP) and Velocity contours have been studied to analyze the combined effect of aneurysms and stenosis in the same arterial network and are compared.

2.3.1 Pressure distribution in healthy and unhealthy condition

(Figure 2.7 (a) & (b)) depict the variation in the pressure distribution along reference line from plane S3 at Z = -0.17 m in healthy and unhealthy (including AAA & RIIAS) of the abdominal artery to the end of outlet Z = -0.36 m during the systolic phase of the cardiac cycle from T_1 to T_6. From the plots in (Figure 2.7 (a)) corresponding to the healthy arterial network, pressure on the inlet region is always higher than that noted at the outlet region of the right iliac artery. It is amply clear that the Central Line pressures (CLPs) significantly vary across the entire arterial network and periodically oscillate with the cardiac cycle. The CLPs which are low at the starting of systole considerably rise up by the mid accelerating systolic phase (T_2) and reaches a maximum at the peak systole (T_3) everywhere, barring a small region close to the right iliac ending, which may be attributed to the asymmetric bifurcation at the right iliac

arterial end under the CT-reconstructed arterial network. By the mid decelerating systolic phase (T_4), the CLPs dip down by more than 50% all over the arterial network, barring the neighborhood region near the outlet of the iliac arteries. By the end of the late systolic phase (T_5, T_6)/early diastolic phase (T_6) the CLPs dip down to a minimum all over the network. It is also to be noted that during the mid-accelerating systolic phase (T_2) and the peak systolic phase (T_3) a considerable fall in CLPs is noticed, especially in the iliac bifurcation region, which is followed by a second and third sharp dips in CLPs in the 1st and 2nd bent/turning regions of the right iliac artery. Such a periodic oscillation in CLP is noticed with progressive cardiac cycles in a healthy arterial network under consideration.

Now the plots in (Figure 2.7 (b)) correspond to the CLPs in a diseased arterial network wherein the pathological complexity due to AAA is further compounded by RIIAS. Here, unlike in the healthy network case, the CLPs are significantly smaller during mid-systolic acceleration (T_2). However, by the peak systole (T_3) they shoot up drastically, in a relatively short time span, to a significantly higher level in the same order as noticed in the healthy network case. It is also seen that, unlike in the healthy case, here CLPs continue to remain as large as peak CLPs during the mid-systolic deceleration time (T_4), which subsequently dips down rapidly by the late systolic (T_5, T_6) or earlier diastolic phase (T_6). Thus, the compounded pathological conditions not only disturb the pressure oscillation rhythm but also bring in rapid variations in CLPs in a much small-time span within a cardiac cycle. It is also to be noted that the peak CLPs, especially in the AAA and RIIAS regions, manifest after the peak systole during the mid-systolic deceleration time. Also, the CLP variations in the region downstream

to the RIIAS are quite different from those in the healthy case throughout the cardiac cycle. It is also to be noted that there is an adverse pressure gradient in the RIIAS region during late systolic and early diastolic phases in the unhealthy case, which can lead to rapid and significant variation in velocity distribution during this phase. Such localized adverse pressure gradient in the RIIAS region is seen to develop during systole and get enhanced by mid-systolic deceleration only to rapidly revert back by late systole (T_5) and finally to reappear again during T_6.

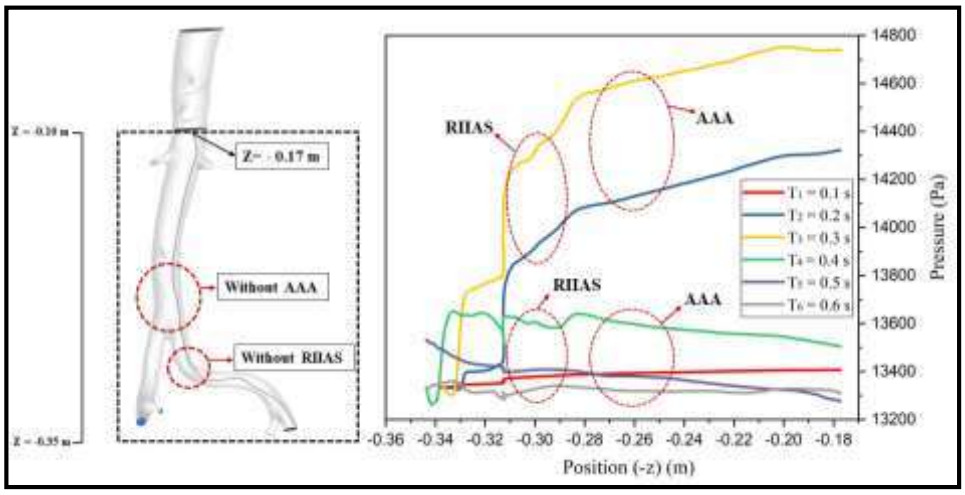

(a)

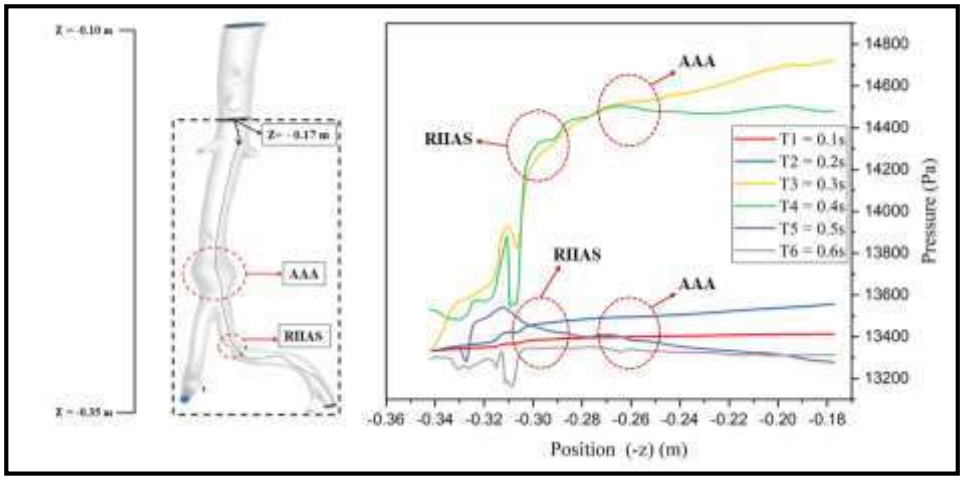

(b)

Figure 2.7: (a) Central Line Pressure distribution along reference line from plane S3 at Z = -0.17 m in healthy abdominal artery to the end of outlet Z = -0.36 m during systolic phase of cardiac cycle from T_1 to T_6 using Newtonian mode (b) Central Line Pressure distribution along reference line from plane S3 at Z = -0.17 m in Unhealthy abdominal artery with (AAA) and (RIIAS) to the end of outlet Z = -0.36 m during systolic phase of cardiac cycle from T_1 to T_6 using Newtonian model.

2.3.2 Velocity profile in healthy and unhealthy artery.

Figure 2.8 (a) & (b) show velocity distribution along the central reference line from plane S3 at Z = -0.17 m in healthy and unhealthy (including AAA & RIIAS) abdominal artery to the end of outlet Z = -0.36 m during the systolic phase of the cardiac cycle from T_1 = 0.1 s to T_6 = 0.6 s using the Newtonian model. In the healthy arterial network case, the maximum velocities are noticed at the peak systolic phase (T_3). But in the case of the diseased vessel, the maximum velocity is attained by the flow during mid decelerating systolic phase (T_4). It is also to be noted that in the diseased arterial network, there is significant variation in the velocities both in AAA and RIIAS regions during the entire flow cycle. While in the healthy arterial network case, the flow velocities, on an average across the entire length of the network, gradually though non-monotonically decrease from the peak systole (T_3) to late systole (T_6) and continue to follow the trend during the early diastolic phase, a marked difference is noticed with the unhealthy case especially during the late systole and early diastole. In the unhealthy case, the velocities, especially in RIIAS region, again shoot up and fall by early diastole, indicating a presence of adverse pressure gradient development in the RIIAS region during late systole. Now a closer look at the CLPs depicted earlier in (Figure

2.8 (b)) does indicate the development of adverse pressure gradient in the RIIAS region during T_6. To ensure such a rapid variation in flow dynamics during late systole and early diastole, simulations are repeatedly carried out, and a detailed flow analysis has also been carried out. The outcome will be presented in the discussion to follow.

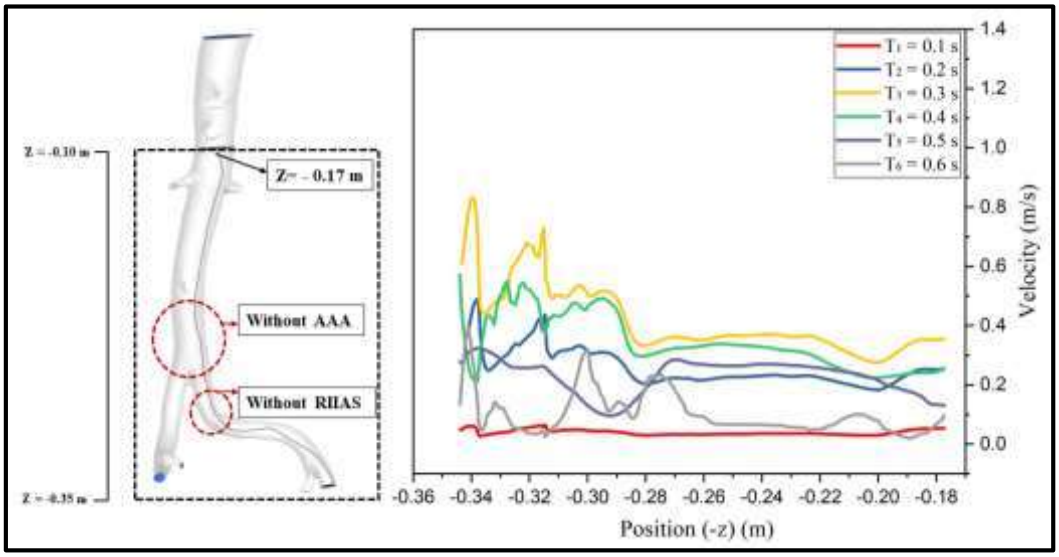

(a)

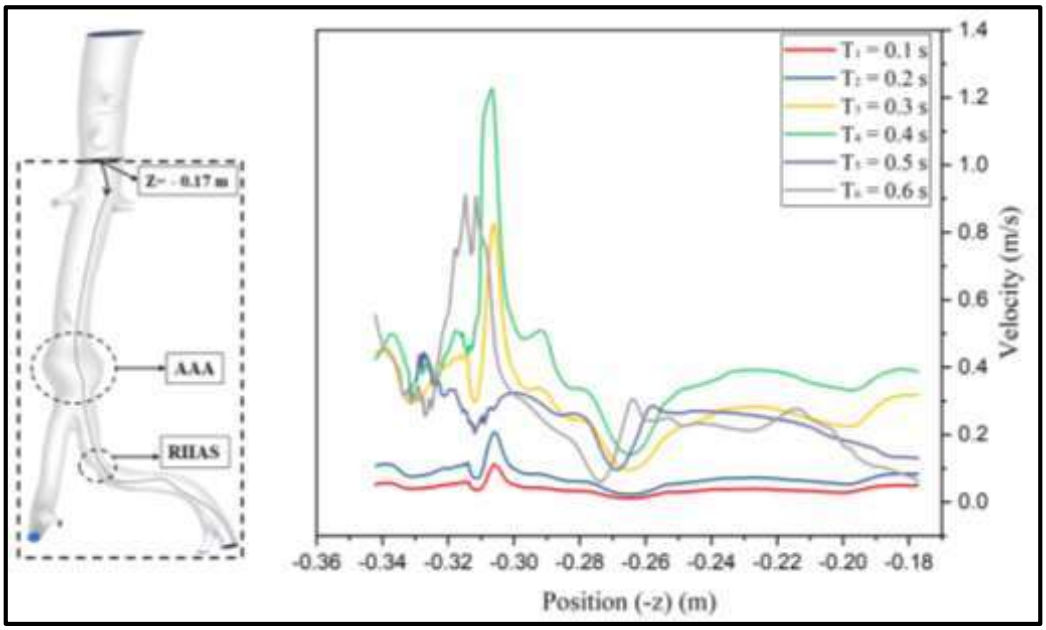

(b)

Figure 2.8 : (a) Velocity distribution along reference line from plane S3 at Z = -0.17 m in healthy abdominal artery to the end of outlet Z = -0.36 m during systolic phase of cardiac cycle from T_1 = 0.1 s to T_6 = 0.6 s using Newtonian model (b) Velocity distribution along reference line from plane S3 at Z = -0.17 m in unhealthy abdominal artery with (AAA) and (RIIAS) to the end of outlet Z = -0.36 m during systolic phase of cardiac cycle from T_1 = 0.1 s to T_6 = 0.6 s using Newtonian model.

2.3.3 Wall Shear Stress (WSS) distribution in healthy and unhealthy artery

2.3.3.1 WSS waveform

WSS distribution along medial wall contour, i.e., on right side of artery from Z = -0.21m in healthy and unhealthy cases covering AAA and RIIAS regions of arterial network till Z = -0.35 m during systolic and early diastolic phases of the cardiac cycle from T_1 = 0.1 s to T_6 = 0.6 s using Newtonian model is presented in (Figure 2.9 (a) & (b)). Generally, in both cases, an oscillation in the WSS during the cardiac cycle is noticed. In the healthy situation, WSS non-monotonically increases across the entire length of the arterial network during the early systolic phase till the peak systole, followed by a similar fall in WSSs in the decelerating systolic phase with a mild oscillatory trend towards the end of systole. This mild oscillation is seen to be sensitive to the arterial lumen dimension, especially near the major bifurcation zone connecting the AA and the iliac arteries. In the unhealthy case, a rapid rise in WSSs is noticed during the second half of the systolic acceleration leading to peak systole, and they continue to remain close to the peak values till the mid systolic deceleration and then have a slow fall till late systole followed by a rapid fall during the systolic-diastolic

transition. It is also to be noted that the WSS magnitudes and their variations are considerably larger in the unhealthy case, especially in the AAA and RIIAS regions than in the healthy case. In the AAA region, the WSSs are lower due to dilation of the vessel wall, and at RIIAS there is a raise is WSS value because of the arterial occlusion. In the RIIAS region, the WSSs are considerably larger on the downstream region, indicating the development flow complexities such as vessel occlusion, separation zone, vortex formation etc. It is also to be noted that in the unhealthy case, the WSSs, especially in RIIAS region during T_6 are relatively larger than during T_5. So as in the velocity and pressure fields, the pathological complexities bring in a rapid second oscillation in WSSs is noticed during the late systole to early diastole phase. It is also to be noted that in the regions corresponding to the head and toe of AAA, WSSs are relatively large through the entire cardiac cycle. Further, it is noticed that in the downstream part of RIIAS, owing to the bending, tapering and upstream occlusion, the WSSs again shoot up. Such a rise is much larger (say, 30% more) in the diseased vessel than that in the healthy one.

2.3.3.2 WSS Contour Distribution

To get a better idea of the WSS distribution on the entire surface of the arterial network, especially during the second half of the systolic cardiac phase, its distribution both in healthy and compounded diseased conditions are depicted in (Figure 2.10 (a-f)) from the peak systole (T_3) to the last systole or the start of diastole (T_6). Clearly, the large WSSs are noticed in the upstream region of the RIIAS during the peak systole in the blood vessel under diseased conditions. During the decelerating systolic large WSSs

are noticed on the downstream region of RIIAS, and subsequently, during the late systole, such large WSSs are noticed further downstream to RIIAS.

2.3.3.3 Local WSS Contour Distribution in unhealthy artery

Now to get an idea on the WSS variation in different sub-sections of the unhealthy arterial network under consideration, WSSs scaled to the sub-sectional local maximum of the network split into three sub-sections are depicted in (Figure 2.11) during the entire cardiac cycle. Clearly, in all the three sub-sections, the sub-section-scaled WSSs are periodically varying with cardiac cycle with peak scaled-WSSs noticed ruing the peak systole. In the upper sub-section corresponding to the descending AA with

Multiple bifurcations in the locally scaled-WSSs are large, especially in bifurcation zones. In the middle sub-section, mainly consisting of AAA, large bands of WSSs are noticed in the head and toe regions of AAA. These large WSS bands manifest during the peak systole and continue to be there, with a reduction in WSS magnitude till late systole. Such large WSS bands, which seem to gradually vanish with systole, reappear during the early diastole only to quickly vanish by the mid- accelerating phase of systole. Hence within a cardiac cycle, while WSSs are periodically varying, they also undergo a rapid secondary second oscillation in AAA region. The last sub-section corresponding to the iliac bifurcation and RIIAS also depict large-scaled-WSSs during peak systole such relatively large-scaled-WSSs continue to be present even till early diastole with a reduced intensity or magnitude. It is to be noted that the scaled-WSSs in the right iliac stenosis zone are relatively more dominating than in the other regions on this sub-section. Such large oscillatory scaled-WSSs noticed both in AAA region

and RIIAS region can get clinically significant. It is now important to further probe this inference from WSSs for its consistency and compatibility from the pressure and flow field distributions too.

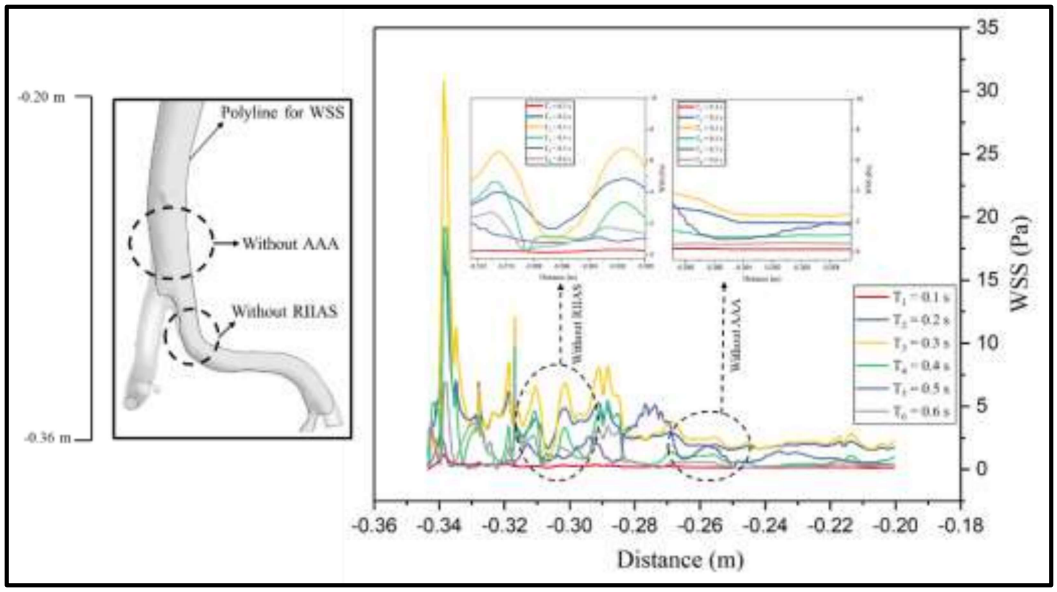

(a)

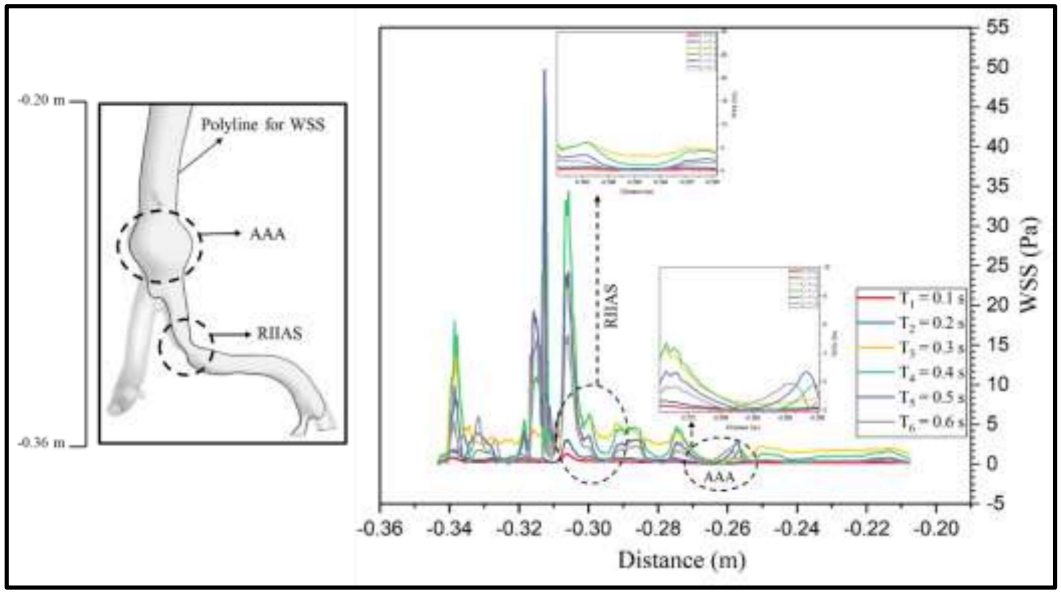

(b)

Figure 2.9 : (a) WSS distribution along medial wall contour i.e., on right side of artery from inlet to the outlet in healthy abdominal artery to the end of outlet Z = -0.36 m during systolic

phase of cardiac cycle from T_1 = 0.1 s to T_6 = 0.6 s using Newtonian model (b) WSS distribution along medial wall contour i.e., on right side of artery from inlet to the outlet in Unhealthy abdominal artery to the end of outlet Z = -0.36 m during systolic phase of cardiac cycle from T_1 = 0.1 s to T_6 = 0.6 s using Newtonian model.

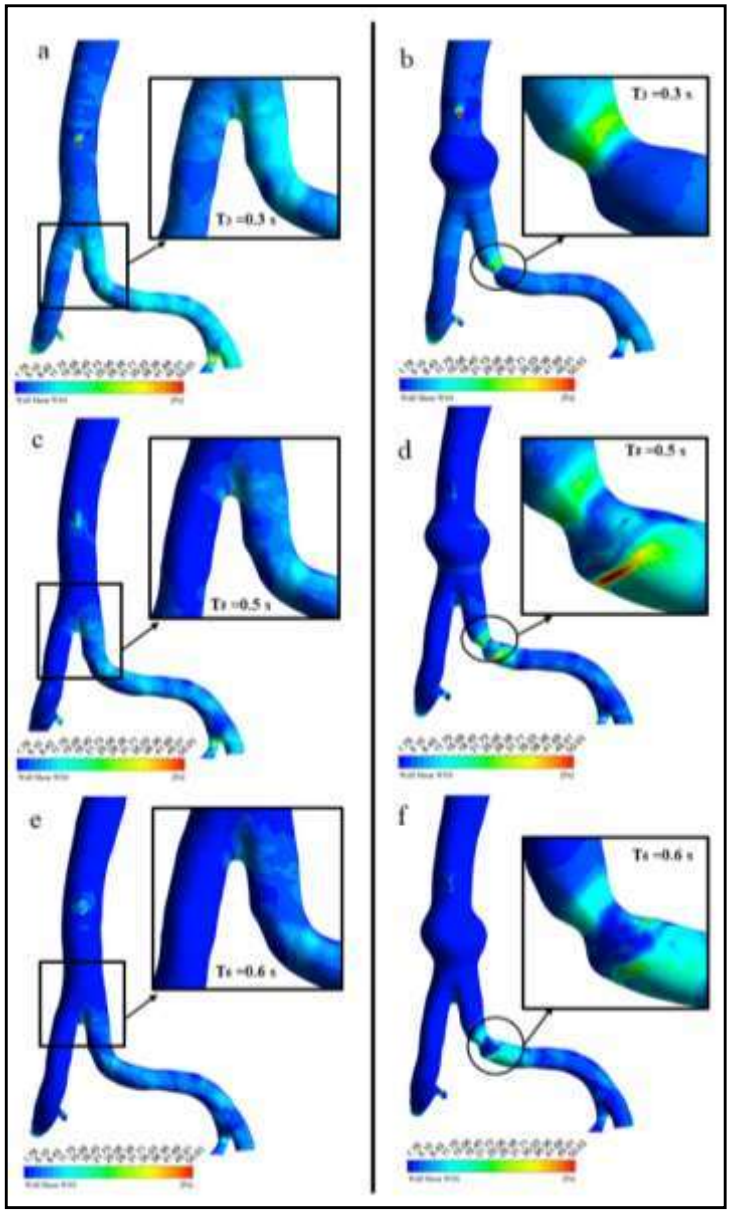

Figure 2.10 : (a) and (b) WSS contour at T_1 of the healthy and unhealthy artery (c) and (d) WSS contour at T_3 of the healthy and unhealthy artery, (e) and (f) WSS contour at T_6 of a healthy and unhealthy artery using Newtonian model.

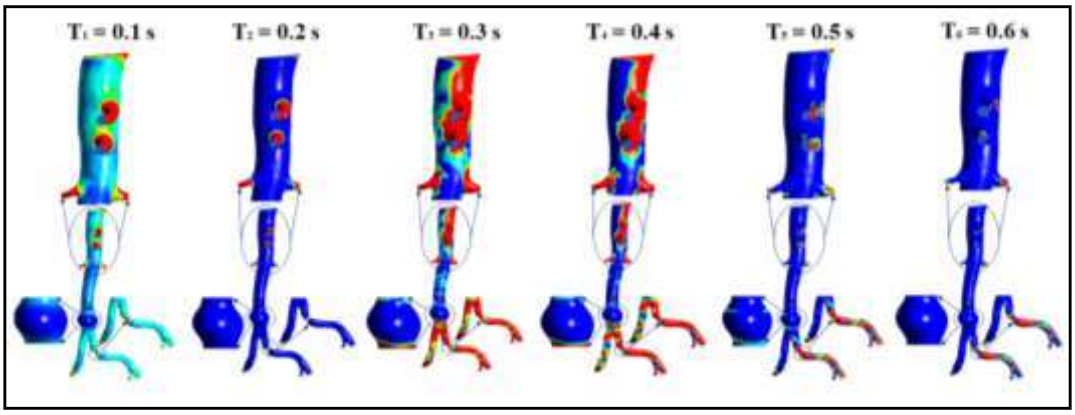

Figure 2.11 : WSS distribution during entire cardiac cycle from T_1 to T_6.

2.3.4 Wall Pressure (WPs) distribution in healthy and unhealthy artery

2.3.4.1 WPs waveform

In (Figure 2.12 (a-b)), the wall pressures (WPs) along the same line as in the WSSs case are presented in (Figure. 2.9 (a) & (b)). The WPs in healthy cases rise to the peak values during the peak systole (T_3) with a rapid increase in the WPs between the early systole (T_1) to mid-accelerating systole (T_2) and a relatively smaller increase during the $T_2 - T_3$ phase. But during the systolic deceleration, a rapid fall in WPs is noticed during the early systolic-decelerating phase ($T_3 - T_4$) than during the late systolic phase ($T_4 - T_5$). Also, an adverse pressure gradient is noticed downstream of the RIIAS region during the late systole cum early diastole. However, the WPs during this period is nearly below that noticed during T_5 along the line of WP measure on the arterial surface. Such WPS are found to periodically repeat with the cardiac beat.

In the unhealthy case, a significantly rapid rise in the WPs is noticed during the second phase of the systolic acceleration, i.e., during ($T_2 - T_3$) with only a small rise in the early systolic acceleration, i.e., during ($T_1 - T_2$) period. Further, during the early

systolic deceleration, i.e., during ($T_3 - T_4$) period, the WPs continue to remain at the peak level, especially in the region downstream of AAA and the upstream of RIIAS (including the leading portion of RIIAS) with local WP oscillations in the downstream region of RIIAS during the systolic deceleration phase. Such adverse pressure gradients and local WP oscillation continue to exist till late systole and stretch into the early diastole. It is also to be noted that in downstream of RIIAS there is local rise and fall in WPs during the ($T_5 - T_6$) cardiac phase. Such complex WP patterns periodically repeat with the heartbeat. Such a WP temporal behavior is in tune with what has been noticed earlier with velocities and WSS. Now it becomes highly desirable to probe further into the WPs on the entire arterial network surface. The WP trace on the entire arterial network surface, especially during the decelerating systole, is presented in (Figure 2.12).

2.3.4.2 WPs contour distribution

In (Figure. 2.13 (a-f)) the WPs contour during the systolic deceleration are presented. Clearly, WPs are seen to be varying across the arterial network wall both in healthy and diseased conditions. During the entire systolic deceleration phase, relatively lower WPs are noticed on the downstream side of the network, baring for a few localized adverse fluctuations in the RIIAS zone and downstream to it. Large pressure bands are also noticed on the toe of the AAA early systolic deceleration phase with a WP dip in the same region during the late systole. Relatively large WPs are noticed on the hull of AAA. Whereas in the healthy case, systolic deceleration WPs are seen to be relatively uniform and less, especially in the region corresponding to AAA.

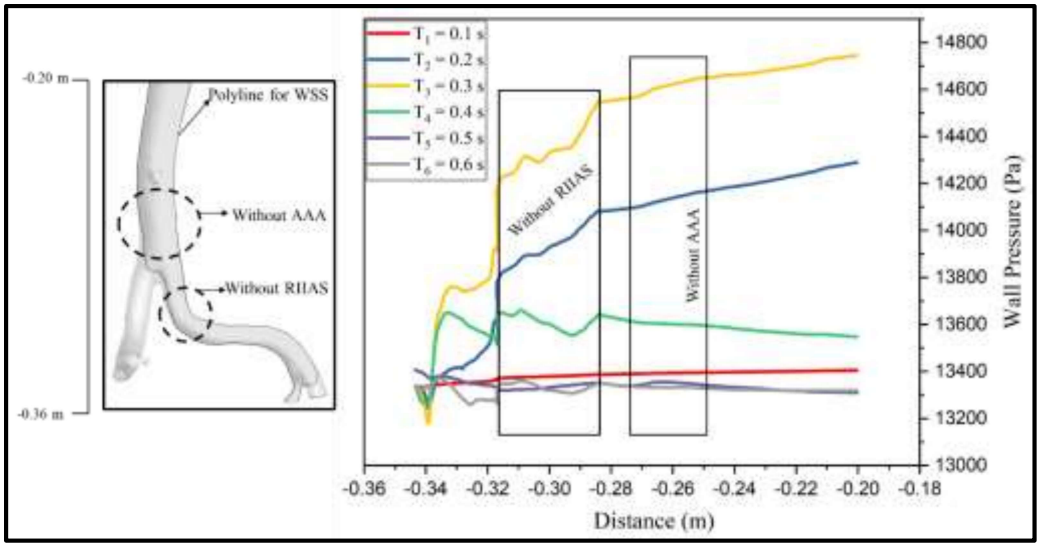

(a)

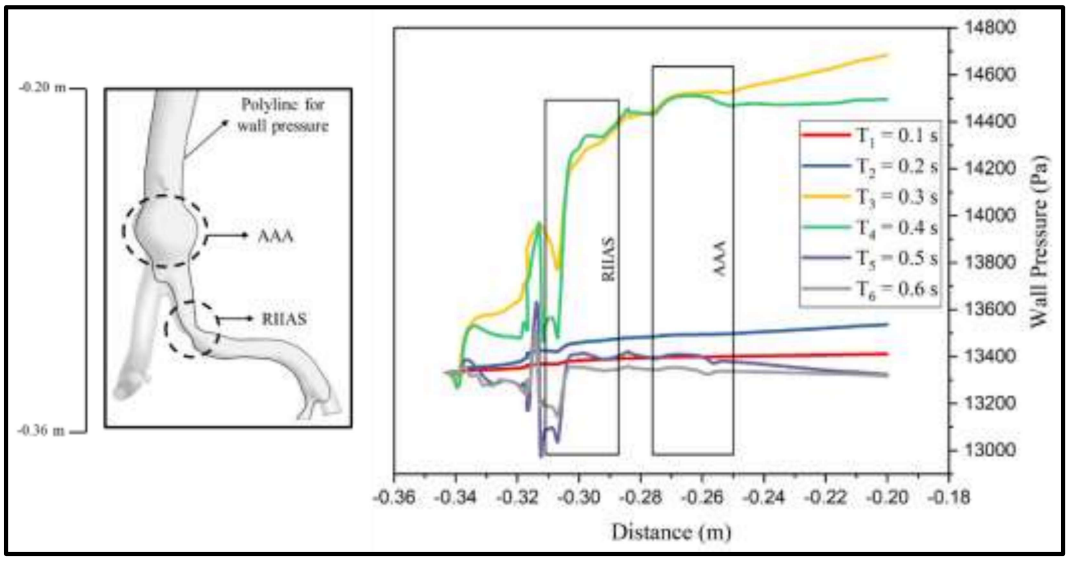

(b)

Figure 2.12 : (a) :- Wall pressure distribution along medial wall contour i.e., on right side of artery from inlet to the outlet in healthy abdominal artery to the end of outlet Z = -0.36 m during systolic phase of cardiac cycle from T_1 = 0.1 s to T_6 = 0.6 s using Newtonian model (b) Wall pressure distribution along medial wall contour i.e., on right side of artery from inlet to the outlet in Unhealthy abdominal artery to the end of outlet Z = -0.36 m during systolic phase of cardiac cycle from T_1 = 0.1 s to T_6 = 0.6 s using Newtonian model.

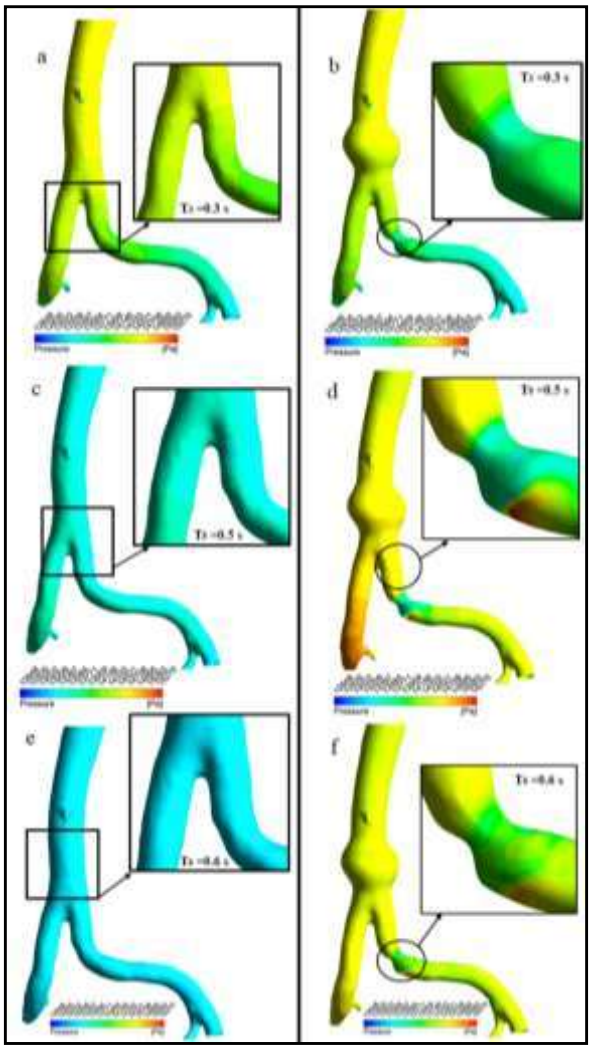

Figure 2.13 : Wall pressure contour during the systolic deceleration phase of cardiac cycle

2.3.5 Streamlines of blood flow during peak of systolic phase

(Figure 2.14) depicts the stream traces of blood flow during the peak systole. The complex pattern of streamlines, recirculation, vorticity and reverse flow behavior during the peak systole are vivid from the plots in the (Figure 2.14). It is to be noted that across the superior medial position of outlets 3 and 4, there is skewness, swirling inflow line and recirculation. Also, across anterior and posterior positions of AAA, intense recirculation zones in the blood flow are seen. Near the inferior RIIAS, randomness in blood flow arises, creating recirculation and reversed flow.

Downstream to RIIAS flow separation zones are noticed. The flow field clearly depicts the complexities arising from the AAA compounded by RIIAS.

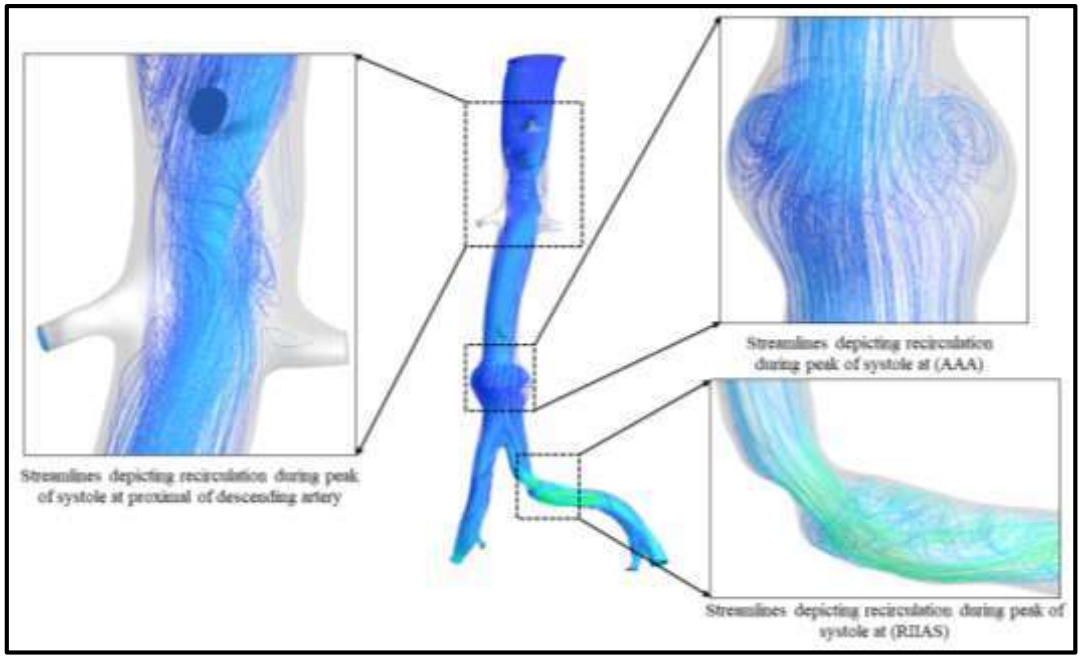

Figure 2.14 : Streamlines of the Newtonian model during peak of systole i.e., at T_3

2.3.6 Core vorticity and Swirling strength distribution

2.3.6.1 Vorticity distribution

Next, a further investigation is made into the flow field. (Figure 2.15) illustrates the three-dimensional vortex core iso-surface at T_3 and T_6 instants of the cardiac cycle. A vortex is instinctively understood as the swirling motion of fluid around a central region of the fluid domain. It is a well-known fact that the amount of vorticity shows energy concentration, circulation conditions and spatial condition of blood dynamics (Contijoch et al., 2020). The (Figure 2.15) shows that iso-vorticity surface dominant at the peak of systole T_3 gets drastically reduced and almost negligible, especially in the region distal to RIIAS by the late systolic period (T_6). Such a feature indicates loss in vorticity due to vortex shedding as depicted earlier in the flow field.

In blood circulation, through the blood vessels, the swirling flow has practical importance as it helps in enhancing oxygen transfer and reduces low-density lipoprotein absorption in the blood vessel by enriching cross-plane mixing of the blood.

2.3.6.2 Swirling strength distribution

(Figure 2.16) depicts the swirling strength at the peak and the end of systole in the cardiac cycle. Clearly, the intensification in flow swirling in the later part of the systolic phase and the development of vortices near the wall region of aneurysms and in pre/post stenotic regions are vivid in the regions enclosed by black circles in Figure 15.

2.3.6.3 Locally scaled axial velocity contour

(Figure 2.17) illustrate the locally scaled velocity contours on the sections S7 and S12 correspond to axial sections at the central portion of AAA and RIIAS. While on S7 corresponding to AAA the maximum variation in scaled velocities across the entire is noticed during the systolic deceleration phase the same is noticed during the systolic acceleration phase on S12 corresponding to RIIAS. It is also to be noted that in the central portion of the S7 the scaled velocities are always large with an asymmetric radial variation in during systole. On S12 the scaled velocities undergo an extreme variation across the entire cross-section during the early systole and only a rapid variation along the boundaries during the decelerating systolic phase. This observation will be helpful during diagnostics while making catheterized measurements.

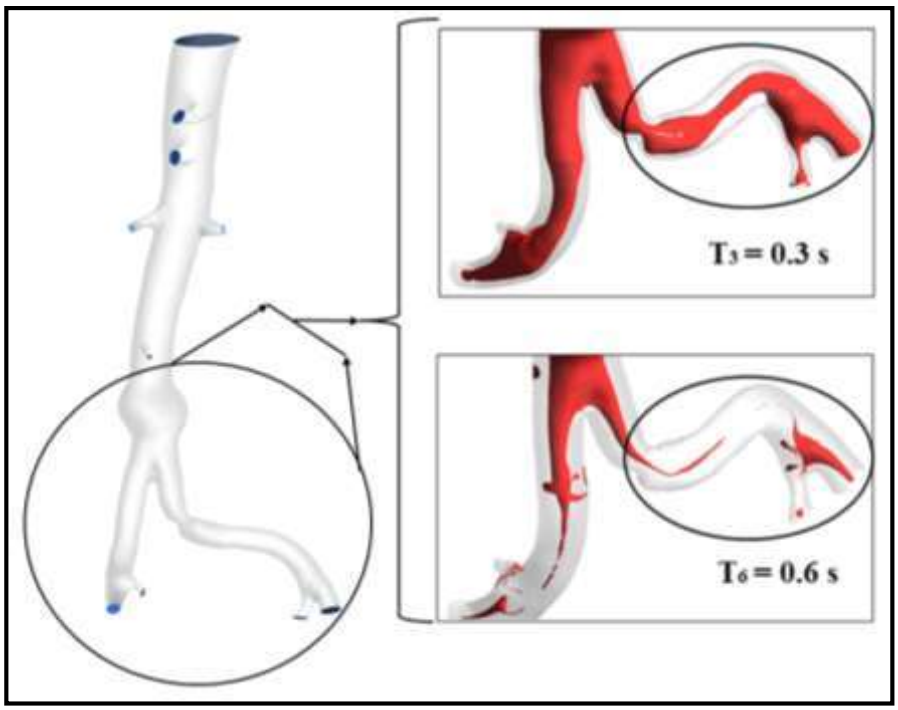

Figure 2.15 : Iso-surface of vorticity core region derived from of cross model during the systolic

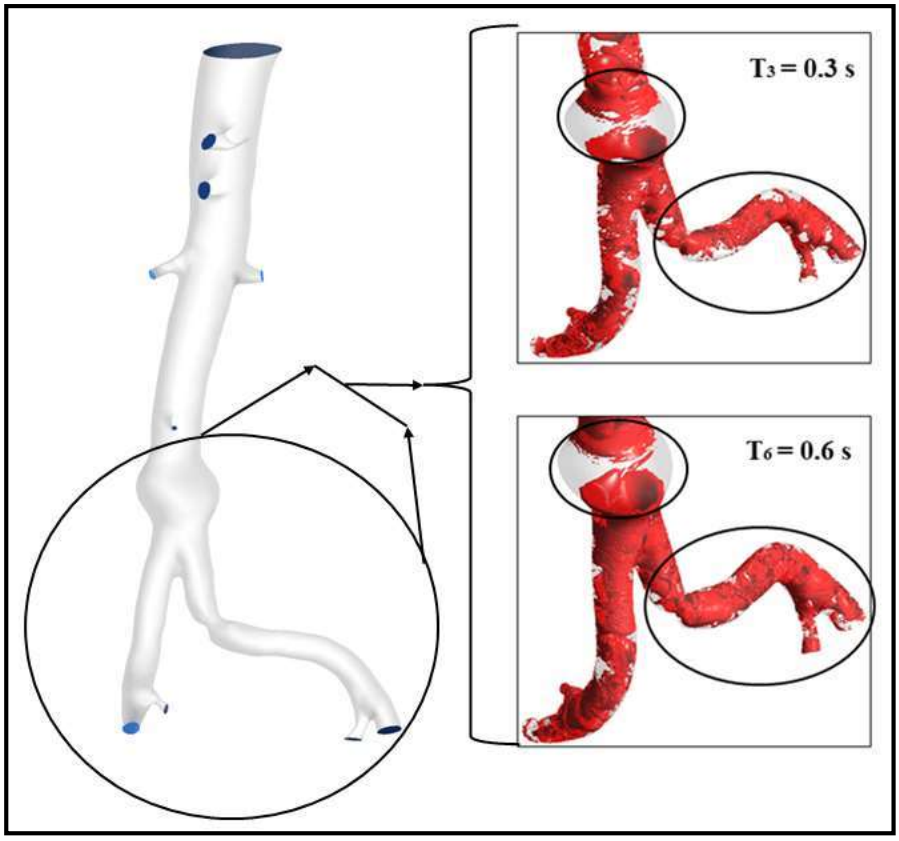

Figure 2.16 : Swirling strength distribution in one cardiac cycle at T_3 and $T_{6=}$ 0.3 and 0.6 s

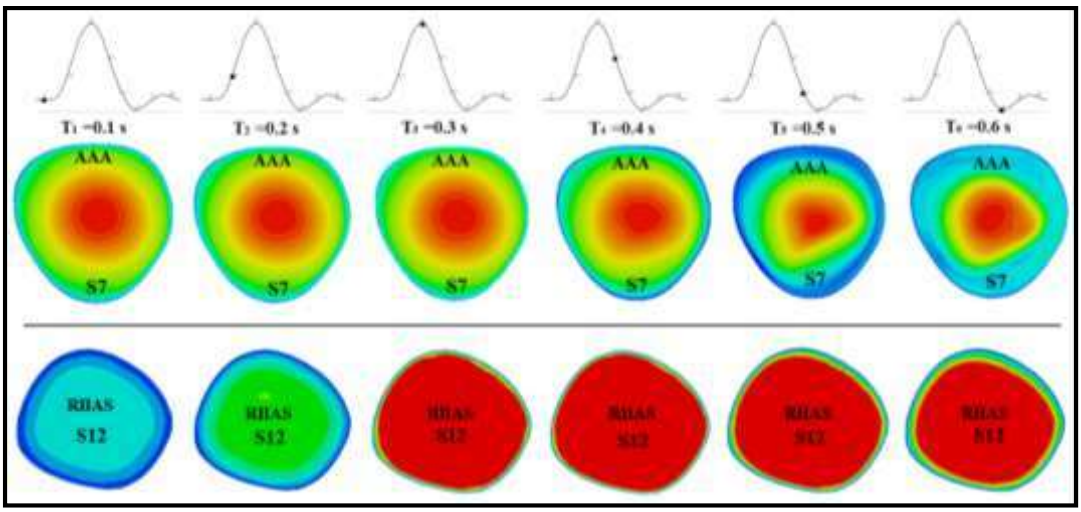

Figure 2.17 : Locally Scaled Velocity Contours on the sections S7 and S12 during the cardiac cycle

2.4 Summary

While earlier studies are focused mainly on ascending abdominal arteries, here, the authors consider the descending abdominal arterial network, which includes AAA and RIIAS and nine outlets, including bifurcations. In this study, using CT scan imaging, a realistic geometry of the artery with AAA and RIIAS is modelled, and pulsatile flow simulations are performed.

- In case of multiple arterial problems like AAA and RIIAS both in the same patient, the blood flow behavior changes in terms of volumetric flow; near the AAA, enhanced blood flow recirculation tendency leading to increased swirling and reversed flow situation. Also, across RIIAS, because of sudden geometric contraction, there is a sudden increase in the maximum velocity. However, just after stenosis, there is waviness or vorticity formation and flow separation as depicted in the streamline plot. This causes a sudden reduction in blood volume in the diseased condition of the iliac artery. This reduced amount of blood flow to the

lower extremities of the human body can cause numbness of the organs in that region.

- The secondary periodic fluctuations with rapid oscillations in flow, pressure, stress fields towards the late systole, especially in the compounded diseased condition, have been consistently observed and seconded by the stream traces, localized adverse pressure gradients, vorticity degeneracy and vigorous swirling in the flow field. Such features put the blood components to additional stress, which can account for the growth in occlusion or generation of multiple occlusions at susceptible new sites downstream to RIIAS or can act as a catalyst for cell leakage that favors thrombus thickening in AAA in the following periods. This is a new insight into hemodynamics under compounded disease conditions.
- The study also traced the effect of arterial vessel bending, tapering and bifurcating through the WSSs, WPs, CLPs, degeneracy in vorticity magnitude and thereby emphasized the consideration of CVD triggered morphological changes to the blood vessels in the clinical diagnostic setting to make CFD based better patient-specific assessment.
- The study also traced the presence of clinically significant high wall shear stress bands and wall pressure bands on the head/toe of the aneurysm during the late phase of systole.
- The D/ La of AAA and D/Ls of RIIAS play an essential role in deciding the diseased portion and its failure predictions. Here in this work, considered percentages are 47% for AAA and 91% for RIIAS. By varying the dilation and

contraction percentage in the same artery, it may affect the mechanical property of the wall.

The current work results in a predictive model that includes some of the detailed anatomic factors that influence abdominal artery blood flow. This work can further extend to various non-Newtonian blood rheology models, fluid-structure interaction with morphological variations to the dimensions of the blood vessel under the pathological conditions, etc.

Chapter 3

Effect of rheological models on pulsatile hemodynamics in a multiply afflicted descending human aortic network

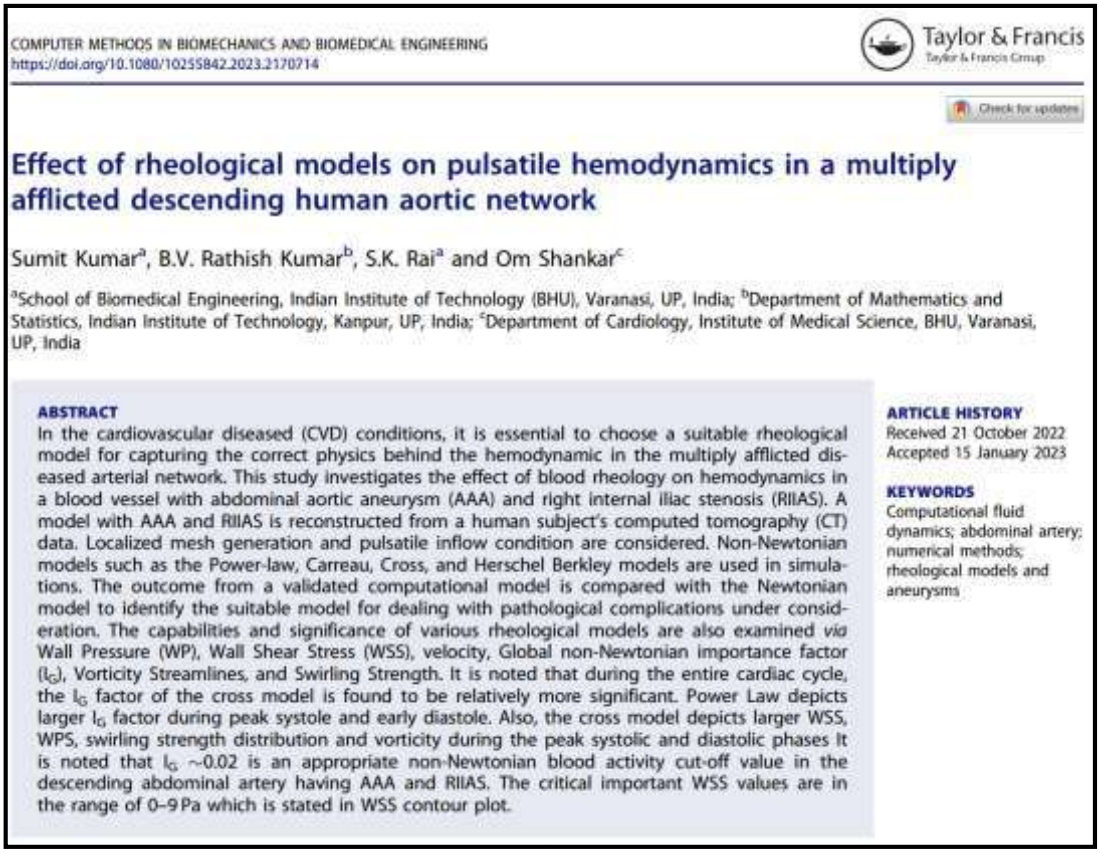

COMPUTER METHODS IN BIOMECHANICS AND BIOMEDICAL ENGINEERING
https://doi.org/10.1080/10255842.2023.2170714

Taylor & Francis
Taylor & Francis Group

Check for updates

Effect of rheological models on pulsatile hemodynamics in a multiply afflicted descending human aortic network

Sumit Kumar[a], B.V. Rathish Kumar[b], S.K. Rai[a] and Om Shankar[c]

[a]School of Biomedical Engineering, Indian Institute of Technology (BHU), Varanasi, UP, India; [b]Department of Mathematics and Statistics, Indian Institute of Technology, Kanpur, UP, India; [c]Department of Cardiology, Institute of Medical Science, BHU, Varanasi, UP, India

ABSTRACT

In the cardiovascular diseased (CVD) conditions, it is essential to choose a suitable rheological model for capturing the correct physics behind the hemodynamic in the multiply afflicted diseased arterial network. This study investigates the effect of blood rheology on hemodynamics in a blood vessel with abdominal aortic aneurysm (AAA) and right internal iliac stenosis (RIIAS). A model with AAA and RIIAS is reconstructed from a human subject's computed tomography (CT) data. Localized mesh generation and pulsatile inflow condition are considered. Non-Newtonian models such as the Power-law, Carreau, Cross, and Herschel Berkley models are used in simulations. The outcome from a validated computational model is compared with the Newtonian model to identify the suitable model for dealing with pathological complications under consideration. The capabilities and significance of various rheological models are also examined *via* Wall Pressure (WP), Wall Shear Stress (WSS), velocity, Global non-Newtonian importance factor (I_G), Vorticity Streamlines, and Swirling Strength. It is noted that during the entire cardiac cycle, the I_G factor of the cross model is found to be relatively more significant. Power Law depicts larger I_G factor during peak systole and early diastole. Also, the cross model depicts larger WSS, WPS, swirling strength distribution and vorticity during the peak systolic and diastolic phases It is noted that I_G ~0.02 is an appropriate non-Newtonian blood activity cut-off value in the descending abdominal artery having AAA and RIIAS. The critical important WSS values are in the range of 0–9 Pa which is stated in WSS contour plot.

ARTICLE HISTORY
Received 21 October 2022
Accepted 15 January 2023

KEYWORDS
Computational fluid dynamics; abdominal artery; numerical methods; rheological models and aneurysms